Geochemical Perspectives Letters

Interaction between clay minerals and organics in asteroid Ryugu

J.-C. Viennet, M. Roskosz, T. Nakamura, P. Beck, B. Baptiste, B. Lavina, E.E. Alp, M.Y. Hu, J. Zhao, M. Gounelle, R. Brunetto, H. Yurimoto, T. Noguchi, R. Okazaki, H. Yabuta, H. Naraoka, K. Sakamoto, S. Tachibana, T. Yada, M. Nishimura, A. Nakato, A. Miyazaki, K. Yogata, M. Abe, T. Okada, T. Usui, M. Yoshikawa, T. Saiki, S. Tanaka, F. Terui, S. Nakazawa, S.-I. Watanabe, Y. Tsuda

Supplementary Information

The Supplementary Information includes:

- Materials and Methods
- Supplementary Information
- Figures S-1 to S-3
- Supplementary Information References

Materials and Methods

Ryugu Grain C-0061

Grain C-0061 of the asteroid Ryugu was provided by the Curation Center at the Extraterrestrial Sample Curation Center, ISAS, JAXA, Japan (P1C). It comes from Chamber C of the Hayabusa2 spacecraft, *i.e.* samples that were collected at the second collection site on the asteroid, close to the ejecta of the SCI artificial crater. The grain was millimetre-scale in size. Half of the grain was cut and sealed in an airtight plastic container in a N_2 atmosphere glove box at the Curation Center.

Smectite Synthesis

Smectite of saponite composition ($Na_{0.4}(Mg_3)[Si_{3.6},Al_{0.4}]O_{10}(OH)_2$) was synthetised from a hydrogel obtained by mixing $Na_2SiO_3 \cdot 5H_2O$ (Sigma Aldrich, >95 %), $AlCl_3 \cdot 6H_2O$ (Sigma Aldrich, 99 %) and $MgCl_2 \cdot 6H_2O$ (Sigma Aldrich, >99 %) in distilled water (18.2 MΩ cm). The hydrogel was mixed at room temperature, then filtered and rinsed (with distilled water) with a vacuum suction filter device. The gel was then placed in 23 mL Teflon reactors and placed in an oven at 230 °C for 4 days, under equilibrium vapor pressure at ~28 Bar. After cooling down, the synthesised smectite was filtered, washed with distilled water and dried at room temperature.

Orgueil Grain

The grain of the Orgueil meteorite was provided by the Museum National d'Histoire Naturelle, Paris, France; it was ~500 µm in diameter.

XRD Measurements

Laboratory X-ray diffraction experiments were performed at the X-ray diffraction facility of the Institut de Minéralogie, de Physique des Matériaux et Cosmochimie (IMPMC), Sorbonne Université (Paris, France). A Rigaku MM007HF diffractometer equipped with Varimax focusing optics, a RAXIS4++ image plate detector placed at a distance of 350 mm from the sample and a Mo rotating anode ($\lambda_{K\alpha1}$ = 0.709319 Å and $\lambda_{K\alpha2}$ = 0.713609 Å) at 50 KeV and 24 mA was used, with a scan range of 3–31 °2θ and the acquisition time of 45 minutes. The *FIT2D* program (Hammersley, 2016) was used for the integration of 2D images into 1D patterns after a calibration using a LaB_6 standard crystalline sample. The XRD beam size was ~70 µm in diameter. In order to ensure that the measurements are representative of the samples, three XRD patterns were taken for each sample and then the final XRD patterns represent the average of the three measurements.

XRD Experiments

XRD experiments under 0 % relative humidity (RH) were carried out using capillary made of borosilicate glass. The grains (Ryugu C-0061, Orgueil) and the synthetic smectite were transferred in a dry glove (<0.5 ppm H_2O and <0.5 ppm O_2) and under 0.9 mbar of Ar atmosphere operating at IMPMC. Then the samples equilibrate with the atmosphere in the glovebox for 1.5 days to allow the desorption of labile the water molecules. Finally, the samples were transferred, in the glove box, into a borosilicate capillary and sealed with cyanoacrylate glue. The sealed capillaries were taken out from the glove box and the XRD measurements were performed immediately after.

Simulation of XRD patterns

The simulated XRD patterns were obtained thanks to the Sybilla software developed by Chevron (Aplin *et al*., 2006). The XRD profile calculation is based on the algorithm initially developed by Sakharov and Drits (1973) and detailed theory of the XRD calculation can be found in Sakharov and Lanson (2013). The program allows to simulate XRD 00ℓ reflections of either pure clay minerals or mixed layers minerals (see Viennet *et al*., 2015, and references therein). Smectite layers were modelled by using a composition of saponite ($n(H_2O) \cdot Ca_{0.15}(Mg_3)[Si_{3.7},Al_{0.3}]O_{10}(OH)_2$). For the simulation, a coherent scattering domain size of 14.8 was chosen for all of the clay phases to avoid apparent irrationality. The dehydrated state was simulated with a saponite layer without water molecule and a layer-to-layer distance of 10.0 Å. The monohydrated state was simulated with a saponite layer with one sheet of water molecules in the middle plane of the interlayer space, a content of 3.5 water molecules per unit cell and a layer-to-layer distance set at 12.5 Å. The bihydrated state was simulated with a layer with two sheets of water molecules in the middle plane of the interlayer space, a content of 3.5 water molecules per unit cell and a layer-to-layer distance set at 15.0 Å. The mixed layer mineral was simulated by using the same layer structures described above with a relative proportion 50 % for each layer and a random stacking defined according to Markovian statistics.

IR Measurements

The IR spectrum of C-0061 shown in Figure 1 was acquired by the MicrOmega hyperspectral imaging instrument installed at the Hayabusa2 Curation Center in Sagamihara (Pilorget *et al*., 2022). It is an average spectrum of the mm-sized grain, thus representative of the bulk composition of C-0061. The spectrum was obtained by averaging spectra from several hundred pixels (each 22 µm wide), acquired in diffused reflectance geometry. Details of the MicrOmega experiment, calibrations and protocols are provided by Riu *et al*. (2022).

Supplementary Information

XRD Measurements of Grain C-0061

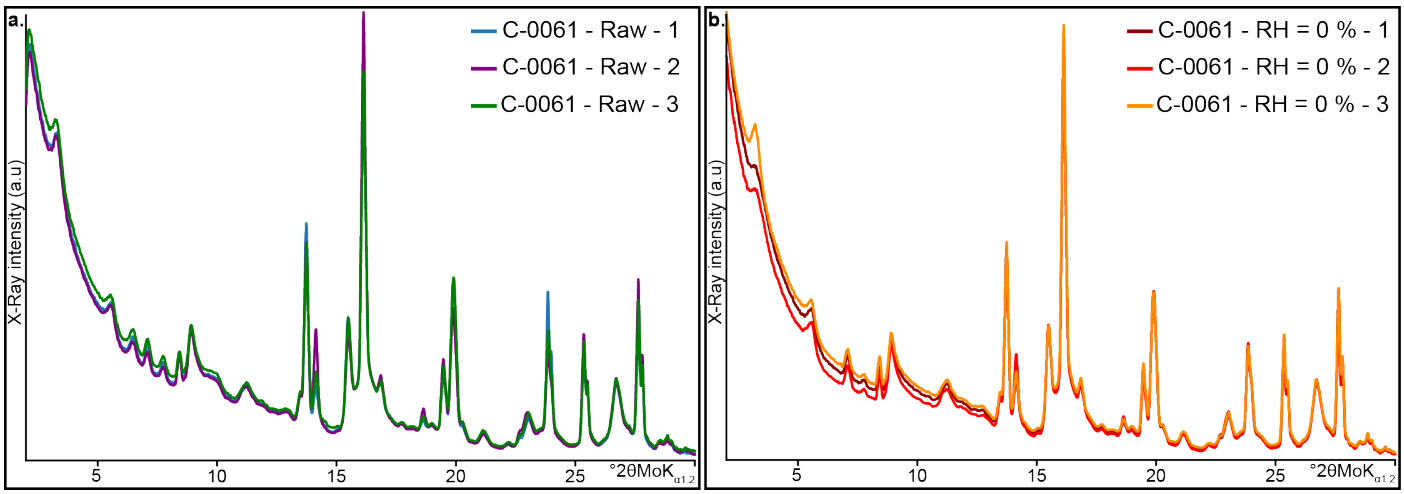

Figure S-1 The three XRD measurements taken on grain C-0061 under **(a)** raw condition and **(b)** 0 % relative humidity (RH).

Structure and Hydration of Smectite Layers

The structure of smectite layer is made of a TOT (T, tetrahedral; O, octahedral) or 2:1 layer and is a part of the family of expandable clay minerals. Isomorphic substitutions in variable amounts by lower charge cations in tetrahedral and/or octahedral sheets induce negatively charged 2:1 layers, the so-called "permanent charge". This permanent charge is in turn compensated by hydrated exchangeable cations in the interlayer space that are responsible for the hydration properties leading to the expansion of the layer-to-layer distance determined by the position of the 001 reflection (Ferrage, 2016). The layer-to-layer distance is dependent on various factors such as the hydration properties of cations, RH or the permanent charge (Ferrage, 2016). Three states of hydrations exist, corresponding to the intercalation of 1, 2, and 3 planes of water molecules in smectite interlayers leading to a monohydrated ($d001$ = 11.6–12.9 Å), a bihydrated ($d001$ = 14.9–15.7 Å), and a trihydrated ($d001$ = 18–19 Å) hydration states, in addition to the dehydrated one ($d001$ = 9.6–10.2 Å) (Ferrage, 2016). Note that, for a given expandable clay mineral and given environmental conditions, different states of hydrations of smectitic layers could occur within the same crystal that leads to mixed layering. For mixed layer minerals, the $\ell \times d00\ell$ product is not constant and the series of 00ℓ reflections is called irrational ($\ell \times d00\ell \neq d001$).

XRD Behaviour of Pure and Mixed Layer Minerals

Figure S-2 shows that for pure clay minerals phases the 00ℓ reflection are rational. For instance, the position of the 001 reflection of the bihydrated smectite is equal to 3 multiplied by the position of the 003 reflection (*i.e.* $d001 = 3 \times d003$, 15.00 Å= 3 × 5.00 Å) and so on for the 004 and 005 reflections. In comparison, for mixed layer minerals, the positions of the series of 00ℓ reflections are irrational (*i.e.* 11.38 Å ≠ 3 × 3.21 Å). Note that the intensity of each XRD pattern correspond to a simulated mixture of 25 % bihydrated smectite, 25 % monohydrated smectite, 25 % dehydrated smectite and 25 % random mixed layer mineral composed of 50 % monohydrated and 50 % dehydrated smectite layers.

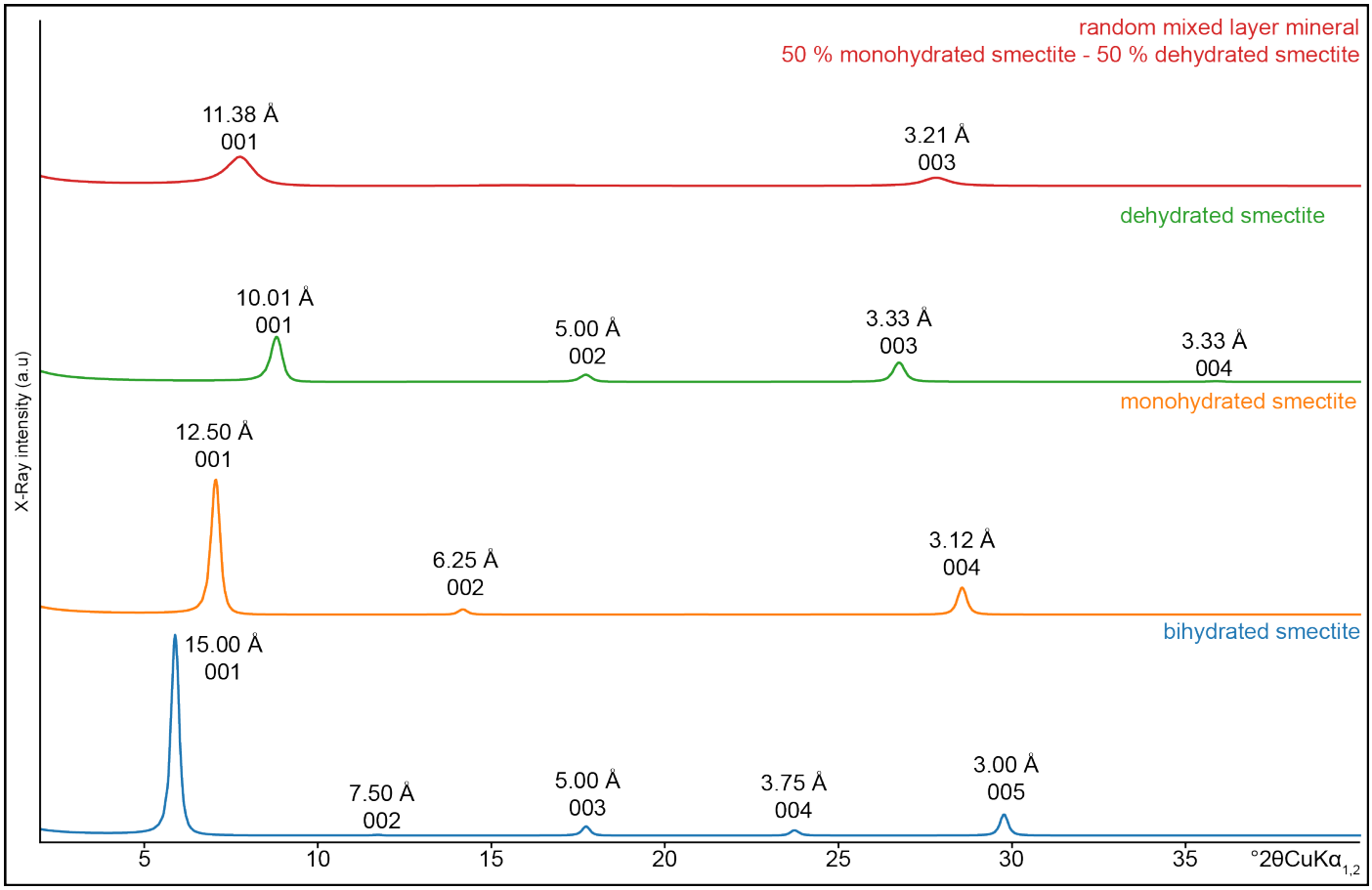

Figure S-2 Simulated X-Ray diffraction patterns showing the position in Angstrom and the 00ℓ for bihydrated, monohydrated, dehydrated smectites and random mixed layer mineral composed of 50 % of monohydrated and 50 % of dehydrated smectite layers.

XRD Experiments on a Reference Synthetic Smectite

A saponite ($Na_{0.4}(Mg_3)[Si_{3.6},Al_{0.4}]O_{10}(OH)_2$) was analysed by XRD in air and then prepared according to the procedure described in the method part. Under 42 % RH (room humidity), the reference smectite presents a 001 reflection at 12.76 Å and a 004 reflection at 3.14 Å (Fig. S-3). The irrationality of the 00ℓ reflections is probably due to both a low coherent scattering domain size (leading to apparent irrationality, shift to lower angle of the 001 reflection) and to mixed layering between monohydrated and bihydrated layers (Ferrage *et al.*, 2010). Hence, such XRD peak positions mainly indicates that smectite has a monohydrated state (Ferrage *et al.*, 2010). After equilibrium under 0 % RH, the 001 reflection shifts to 10.43 Å and its 003 reflection shift at 3.25 Å. Again, the irrationality of the 00ℓ reflections could be attributed to both a low coherent scattering domain size and mixed layering between dehydrated and monohydrated layers (Ferrage *et al.*, 2010). Typically, such XRD peak positions correspond mainly to dehydrated smectite (Ferrage *et al.*, 2010). We note that the 004 reflection of dehydrated smectite and the 003 reflection of monohydrated smectite are not detectable on our reference synthetic material due to the structural factor of smectite that leads to low or absence of such reflection (such XRD behaviours are illustrated in the simulated XRD patterns for smectite in Fig. S-2). This reference experiment demonstrates the efficient removal of the water molecules from the interlayer space of smectites.

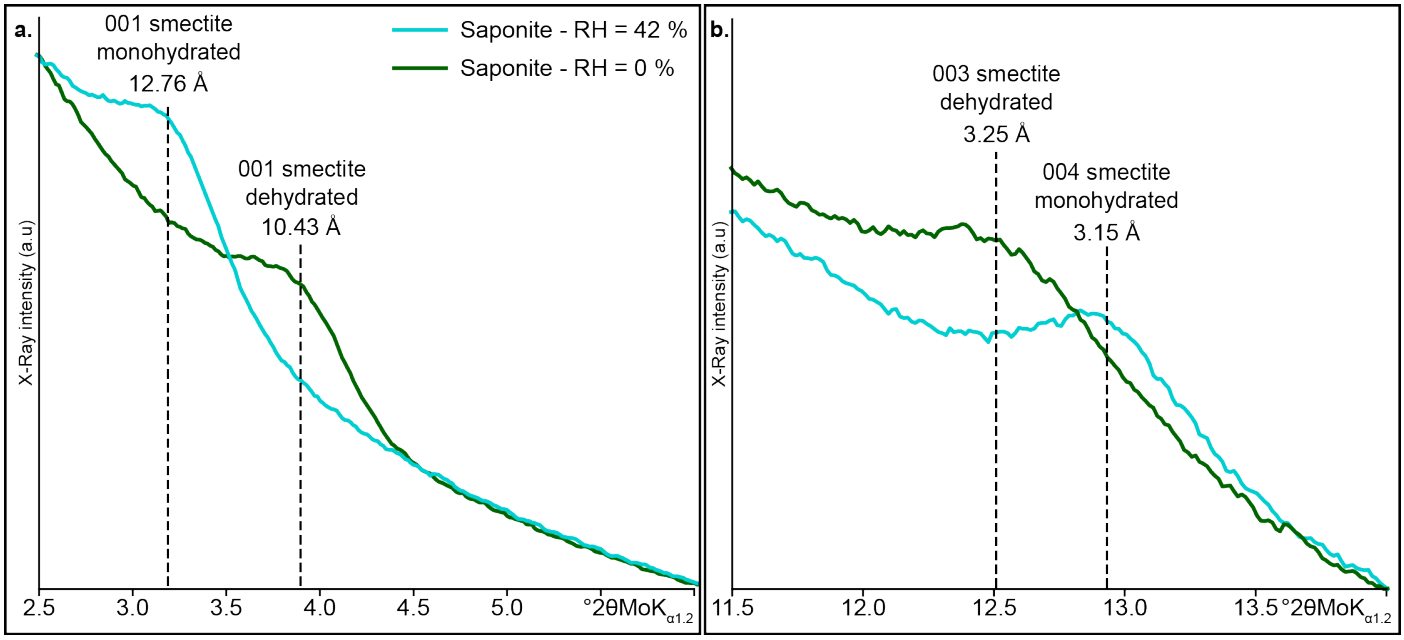

Figure S-3 XRD measurements and the corresponding peak assignation of the 00ℓ reflections of the synthetic smectite under 42 % and 0 % RH conditions for **(a)** 001 reflections and **(b)** 003 and 004 reflections of smectite.

Supplementary Information References

Aplin, A.C., Matenaar, I.F., McCarty, D.K., van der Pluijm, B.A. (2006) Influence of Mechanical Compaction and Clay Mineral Diagenesis on the Microfabric and Pore-Scale Properties of Deep-Water Gulf of Mexico Mudstones. *Clays and Clay Minerals* 54, 500–514. https://doi.org/10.1346/CCMN.2006.0540411

Ferrage, E. (2016) Investigation of the Interlayer Organization of Water and Ions In Smectite from the Combined Use of Diffraction Experiments And Molecular Simulations. A Review of Methodology, Applications, And Perspectives. *Clays and Clay Minerals* 64, 348–373. https://doi.org/10.1346/CCMN.2016.0640401

Ferrage, E., Lanson, B., Michot, L.J., Robert, J.-L. (2010) Hydration Properties and Interlayer Organization of Water and Ions in Synthetic Na-Smectite with Tetrahedral Layer Charge. Part 1. Results from X-ray Diffraction Profile Modeling. *The Journal of Physical Chemistry C* 114, 4515–4526. https://doi.org/10.1021/jp909860p

Hammersley, A.P. (2016) *FIT2D*: a multi-purpose data reduction, analysis and visualization program. *Journal of Applied Crystallography* 49, 646–652. https://doi.org/10.1107/S1600576716000455

Pilorget, C., Okada, T., Hamm, V., Brunetto, R., Yada, T., *et al*. (2022) First compositional analysis of Ryugu samples by the MicrOmega hyperspectral microscope. *Nature Astronomy* 6, 221–225. https://doi.org/10.1038/s41550-021-01549-z

Riu, L., Pilorget, C., Hamm, V., Bibring, J.-P., Lantz, C., *et al*. (2022) Calibration and performances of the MicrOmega instrument for the characterization of asteroid Ryugu returned samples. *Review of Scientific Instruments* 93, 054503. https://doi.org/10.1063/5.0082456

Sakharov, B.A., Drits, V.A. (1973) Mixed-Layer Kaolinite-Montmorillonite: A Comparison of Observed and Calculated Diffraction Patterns. *Clays and Clay Minerals* 21, 15–17. https://doi.org/10.1346/CCMN.1973.0210104

Sakharov, B.A., Lanson, B. (2013) Chapter 2.3 - X-ray Identification of Mixed-Layer Structures: Modelling of Diffraction Effects. In: Bergaya, F., Lagaly, G. (Eds.) *Developments in Clay Science 5, Handbook of Clay Science*. Elsevier, Amsterdam, 51–135. https://doi.org/10.1016/B978-0-08-098259-5.00005-6

Viennet, J.-C., Hubert, F., Ferrage, E., Tertre, E., Legout, A., Turpault, M.-P. (2015) Investigation of clay mineralogy in a temperate acidic soil of a forest using X-ray diffraction profile modeling: Beyond the HIS and HIV description. *Geoderma* 241–242, 75–86. https://doi.org/10.1016/j.geoderma.2014.11.004